Polymer Journal (2016) 48, 729–739

www.nature.com/pj

ORIGINAL ARTICLE

Morphological control of hybrid amphiphilic poly(*N*-isopropylacrylamide)/metal cyanide complexes

Keita Kuroiwa[1], Yuko Koga[1], Yuya Ishimaru[1], Takuya Nakashima[2], Hiroshi Hachisako[1] and Shinichi Sakurai[3]

A number of amphiphilic *N*-isopropylacrylamide (NIPAAm) oligomers and polymers with a *S*-1-dodecyl-*S*′-trithiocarbonate (DTC) and an amino terminal group were prepared using RAFT polymerization: DTC-NIPAAm$_{13}$-NH$_3$Cl (1), DTC-NIPAAm$_{61}$-NH$_3$Cl (2), DTC-NIPAAm$_{78}$-NH$_3$Cl (3), DTC-NIPAAm$_{119}$-NH$_3$Cl (4). and DTC-NIPAAm$_{274}$-NH$_3$Cl (5). Aqueous solutions of 1–5 became cloudy upon heating at pH 10, while 1–4 did not exhibit thermosensitivity at pH 7.0, instead forming stable rods and vesicles in aqueous solution. Nanorods and nanosquares were obtained from metal cyanide complexes of 1 and 2, both of which had low degrees of polymerization, and aqueous solutions of these nanocomposites became cloudy at pH 7.0. The electrostatic interactions between the amine segments and the anionic metal cyanide complexes as well as the low degree of polymerization in the vicinity of approximately 100 were both found to have a significant role in the morphology and thermoresponsiveness of the hybrids. These hybrid NIPAAm oligomer/metal cyanide complexes may allow the design of flexible, functional supramolecular systems in aqueous solutions.
Polymer Journal (2016) **48,** 729–739; doi:10.1038/pj.2016.13; published online 17 February 2016

INTRODUCTION

Many researchers have investigated nanocomposites composed of polymers and inorganic compounds because such composites offer control over the molecular structure and an associated tunability of specific morphological, chemical and physical properties.[1] In particular, significant work has been performed with regard to the development of nanocomposites of polymers and functional inorganic molecules, such as metal nanoparticles,[2,3] metal oxides (made via sol–gel methods)[4,5] and metal salts.[6] In addition, the hierarchical assembly and highly ordered alignment of such materials may lead to much higher functionalization, with applications in electronics[7–11] and optics,[12–16] as well as in materials separation.[17,18] This class of nanocomposites built around the self-assembly of polymers and inorganic compounds has become a significant area of focus within the study of polymeric and supramolecular materials based on element blocks.[19]

Nanocomposites that incorporate metal complexes are important materials that often display functional properties owing to the coordination of inorganic molecules with organic ligands and the resulting formation of various electronic states.[20–25] In our previous research, the interactions between metal complexes have been controlled dynamically via self-assembling structures and nano-architectures, leading to specific morphological and spectroscopic behaviors. In such work, the precise control of the interactions among metal complexes, such as metalloproteins and enzymes, was readily controlled through stimuli-responsive polymer counterparts, which endow nanocomposites with dynamic and flexible switching capabilities.[23–25]

It is well known that poly(*N*-isopropylacrylamide) (PNIPAAm) exhibits a significant and abrupt thermal transition at its lower critical solution temperature (LCST).[26,27] For this reason, PNIPAAm synthesized by living polymerization has been used to develop highly ordered functional materials showing thermoresponsiveness.[26–32] For example, thermoresponsive hybrids of PNIPAAm with inorganic compounds, such as gold nanoparticles,[33–41] gold nanocages,[42] silver nanoparticles,[43] magnetic nanoparticles,[44–47] silica nanoparticles[48–50] and silsesquioxanes,[51–54] have been developed with the aim of producing functional organic/inorganic nanomaterials. In addition, copolymers of PNIPAAm with acrylic acid,[55] carboxylates,[56] crown ethers,[57] aza crowns,[58] polythioethers,[59] phenanthoroline,[60] terpyridine[61] and iminodiacetic acid derivatives[62] have been synthesized to tune the LCST transition and achieve the extraction and recognition of metal ions. However, there have been no reports on controlling the alignment of metal complexes in these materials. Ideally, the characteristics of such metal complexes would be manipulated by controlling the spatial arrangement of complexes within the composite, resulting in supramolecular nanocomposites without covalent or coordinative linkages.

In the present work, we focus on the self-assembly mechanism in nanocomposites composed of amphiphilic NIPAAm oligomers and polymers with metal complexes to allow the hierarchical control of morphology. Amphiphilic polymers are commonly used to obtain various nanoarchitectures, including vesicles and micelles.[63,64]

[1]Department of Nanoscience, Faculty of Engineering, Sojo University, Kumamoto, Japan; [2]Graduate School of Materials Science, Nara Institute of Science and Technology, NAIST, Nara, Japan and [3]Department of Biobased Materials Science, Kyoto Institute of Technology, Kyoto, Japan
Correspondence: Dr K Kuroiwa, Department of Nanoscience, Faculty of Engineering, Sojo University, 4-22-1 Ikeda, Nishi-ku, Kumamoto 860-0082, Japan.
E-mail: keitak@nano.sojo-u.ac.jp
Received 31 August 2015; revised 10 December 2015; accepted 13 December 2015; published online 17 February 2016

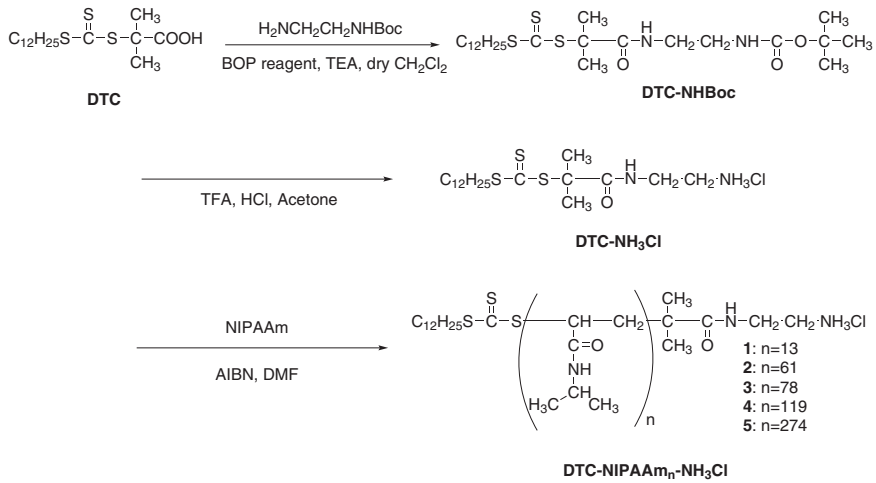

Figure 1 Synthesis of amphiphilic PNIPAAms from DTC by modification of procedures previously published in the literature.

In addition, we make it increasingly clear that amphiphilic NIPAAm oligomers with LCST can form molecular hybrids with inorganic components, such as metal ions.[25] In this study, we concentrate specifically on macromolecules at the transition point between oligomers and polymers, with a degree of polymerization of approximately 100, as well as on inorganic compounds with the ability to self-aggregate, to exhibit metal–metal interactions and to form one- or two-dimensional (2-D) assemblies. These oligomeric/polymeric NIPAAm amphiphiles were integrated with metal complexes and the morphological regulation and transformation and thermodynamic control of the resulting composites were assessed.

EXPERIMENTAL PROCEDURE

Materials

Reagents and solvents were obtained from various commercial sources (Kanto Chemical Co. Inc., Tokyo, Japan, Sigma-Aldrich Chemical Co. LLC., St Louis, MO, USA, Nacalai Tesque, Inc., Kyoto, Japan, Wako Pure Chemical, Ltd., Osaka, Japan, Tokyo Chemical Industry Co., Ltd., Tokyo, Japan, Junsei Chemical Co., Ltd., Tokyo, Japan) and used without further purification unless otherwise noted. Pyrogen-free deionized (DI) water was obtained from Advantec RFD240NA and RFU655DA purification units (Advantec Toyo Kaisha, Ltd., Tokyo, Japan). Anhydrous dimethylformamide was obtained by distillation over $CaCl_2$ while purging with nitrogen. NIPAAm and 2,2′-azobisbutylonitrile were purified by recrystallization from ethanol solution.

Instrumentation

The structures of oligomers and polymers were confirmed by thin-layer chromatography, Fourier Transform Infrared (FT-IR; Perkin Elmer, Inc., Waltham, MA, USA, Spectrum 65) and ^{1}H nuclear magnetic resonance (NMR; JEOL, Ltd., Tokyo, Japan, ESC 400, 400 MHz) spectroscopy and elemental analysis. Ultraviolet–visible (UV-vis) and fluorescence spectra were acquired using RF-2500PC and RF-5300PC spectrophotometers, respectively (Shimadzu Co., Ltd., Kyoto, Japan). Transmission electron microscopy (TEM) was performed with a Tecnai G2 F20 instrument (FEI Co., Hillsboro, OR, USA) operating at 200 kV. TEM specimens were prepared by putting a carbon-coated TEM grid on the liquid surface of a solution, removing the TEM grid and transferring the nanostructure in solution onto the carbon-coated TEM grid. Assessments using 2-D small-angle X-ray scattering (SAXS)[65] with high brilliance synchrotron X-rays were carried out using a PILATUS300K-W (Dectris Ltd., Baden, Switzerland; 2-D detector), applying a wavelength of 0.1488 nm, on the BL-10C beamline at the Photon Factory within the High Energy Accelerator Research Organization, Tsukuba, Japan. Chicken tendon collagen was used as a standard sample for SAXS measurements to calibrate the magnitude of the scattering vector, q, as defined by $q = (4\pi/\lambda)\sin(\theta/2)$, with λ and θ being the X-ray wavelength and scattering angle, respectively. The 2-D SAXS patterns were further converted to one-dimensional profiles by sector averaging. Emission quantum yields were determined using a Hamamatsu C9920-02 instrument (excitation: 355 nm) (Hamamatsu Photonics K.K., Shizuoka, Japan), and phosphorescence lifetimes were assessed using the time-correlated single-photon counting method with a Horiba FluoroCube 3000U (excitation: 340 nm, nano LED, repetition rate: 100 kHz) (HORIBA, Ltd., Kyoto, Japan).

Synthesis of the chain transfer agent, *S*-1-dodecyl-*S*′-(α,α′-dimethyl-α″-acetic acid)trithiocarbonate (DTC) and *S*-1-dodecyl-*S*′-(α,α′-dimethyl-α″-(*N*-(2-aminoethyl)acetamide)trithiocarbonate chloride (DTC-NH_3Cl)

DTC was synthesized according to a literature procedure,[66] and DTC-NH_3Cl was obtained from DTC by modified literature procedures (Figure 1).[67–70]

A solution of DTC (3.3 g, 8.9 mmol) and ((benzotriazol-1-yloxy)-tris(dimethylamino) phosphonium hexafluorophosphate (4.60, 10 mmol) in dry dichloromethane was degassed by sparging with N_2. *N*-Boc-ethylenediamine (1.0 g, 6.2 mmol) in 10 ml dichloromethane was added dropwise to the solution, followed by the dropwise addition of dry trimethylamine (0.6 ml, 6.0 mmol). During these additions, the solution temperature was maintained at 0 °C. The mixture was subsequently stirred for 43 h; washed with an aqueous $NaHCO_3$ solution (×3), a saturated aqueous NaCl solution (×3) and brine and finally dried over Na_2SO_4. Chromatographic separation (Silica gel, petroleum ether/ethyl acetate (10:9, v/v)) yielded DTC-NHBoc as a yellow oil (2.6 g, 82%). DTC-NHBoc: FT-IR (attenuated total reflectance (ATR)): ν_{max} cm^{-1} 3334, 1692, 1657, 1515, 1066, 732; ^{1}H NMR ($CDCl_3$ with 0.05% v/v TMS, 400 MHz): δ_H 0.86–0.90 (3H, t, $J = 6.0$ Hz, $CH_3(CH_2)_8-$), 1.15–1.35 (16H, m, $CH_3(CH_2)_8$), 1.38–1.40 (2H, m, $CH_2CH_2CH_2S$), 1.44 (9H, s, $C(CH_3)_3$), 1.63–1.66 (2H, m, CH_2CH_2S), 1.69 (6H, s, $SC(CH_3)_2CO$), 3.26–3.33 (2H, m, CH_2S) and (4H, m, $NHCH_2CH_2NH$), 4.79 (1H, m, NHCOO), 6.88 (1H, m, $C(CH_3)_3CONH$).

DTC-NHBoc (2.6 g, 5.1 mmol) was dissolved in trifluoroacetic acid (18 ml) at 0 °C. After stirring for 1.5 h, the solution was concentrated under vacuum and dissolved in acetone (42.3 ml). Holding the solution temperature at 0 °C, concentrated hydrochloric acid (0.77 ml) was slowly added dropwise, after which the solution was stored overnight in a refrigerator. The resulting precipitate was removed by filtration and dissolved in ethanol (50 ml). The ethanol solution was then added to n-hexane (800 ml), producing a yellow solid (2.9 g, 73%). DTC-NH_3Cl: FT-IR (ATR): ν_{max} cm^{-1} 3416–3347, 1646, 1637, 1529, 1061, 722; ^{1}H NMR ($CDCl_3$ with 0.05% v/v TMS, 400 MHz): δ_H 0.86–0.90 (3H, t, $J = 6.4$ Hz, $CH_3(CH_2)_8-$), 1.15–1.35 (16H, m, $CH_3(CH_2)_8$), 1.37–1.38 (2H, m, $CH_2CH_2CH_2S$), 1.63–1.68 (2H, m, CH_2CH_2S), 1.73 (6H, s, $SC(CH_3)_2CO$), 3.21–3.23 (2H, m, CH_2S), 3.25–3.29 (2H, m, $NHCH_2CH_2NH_3Cl$), 3.62–3.63 (2H, m, $NHCH_2CH_2NH_3Cl$), 7.52–7.57 (1H, m, $C(CH_3)_3CONH$).

Table 1 Results from the polymerization of DTC-NH_3Cl and NIPAAm

Sample	*NIPAAm per g (mmol)*	*DTC-NH_3Cl per g (mmol)*	*AIBN per g (mmol)*	*Degree of polymerization of NIPAAm (M_n)*	*Mw/Mn*	*Yield per g*	*Conv./%*
1: DTC-NIPAAm$_{13}$-NH_3Cl	0.17 (1.5)	0.067 (0.15)	0.028 (0.17)	13 (1900)	1.03	0.099	57
2: DTC-NIPAAm$_{61}$-NH_3Cl	0.28 (2.5)	0.22 (0.55)	0.083 (0.50)	61 (7300)	1.13	0.21	75
3: DTC-NIPAAm$_{78}$-NH_3Cl	0.57 (5.0)	0.22 (0.55)	0.083 (0.51)	78 (9200)	1.06	0.45	79
4: DTC-NIPAAm$_{119}$-NH_3Cl	1.1 (12)	0.21 (0.50)	0.82 (5.0)	119 (13 900)	1.20	0.79	71
5: DTC-NIPAAm$_{274}$-NH_3Cl	0.93 (8.2)	0.073 (0.16)	0.027 (0.16)	274 (31 400)	1.16	0.53	57

Abbreviations: AIBN, 2,2′-azobisbutylonitrile; DTC-NH_3Cl, *S*-1-dodecyl-*S*′-(α,α′-dimethyl-α″-(*N*-(2-aminoethyl)acetamide)trithiocarbonate chloride; NIPAAm, *N*-isopropylacrylamide.

Table 2 LCST (°C) of DTC-NIPAAm$_n$-NH_3Cl (1–6) in aqueous solution at various pH

Sample	*pH 3.0*	*pH 4.0*	*pH 5.0*	*pH 6.0*	*pH 7.0*	*pH 8.0*	*pH 9.0*	*pH 10.0*	*pH 11.0*
1: DTC-NIPAAm$_{13}$-NH_3Cl	NA	NA	NA	NA	NA	NA	27	28	30
2: DTC-NIPAAm$_{61}$-NH_3Cl	NA	NA	NA	NA	NA	NA	NA	4	4
3: DTC-NIPAAm$_{78}$-NH_3Cl	NA	NA	NA	NA	NA	NA	NA	11	14
4: DTC-NIPAAm$_{119}$-NH_3Cl	NA	NA	NA	NA	NA	NA	28	28	27
5: DTC-NIPAAm$_{274}$-NH_3Cl	31	31	31	31	29	28	28	28	28

Abbreviations: DTC, *S*-1-dodecyl-*S*′-trithiocarbonate; LCST, lower critical solution temperature; NA, distinct LCST (phase separation) was not observed; NIPAAm, *N*-isopropylacrylamide.

Synthesis of amphiphilic PNIPAAm

Amphiphilic PNIPAAm was synthesized using reversible addition-fragmentation chain transfer polymerization (RAFT), following a literature procedure.[28] The paragraph below describes a typical polymerization of NIPAAm under bulk conditions at 70 °C employing an amphiphilic PNIPAAm derived from DTC (Table 1 lists the amounts of all reagents).

NIPAAm, 2,2′-azobisbutylonitrile and DTC-NH_3Cl (see Table 1) were added to a 50.0 ml round-bottom flask equipped with a magnetic stir bar, after which the solution was degassed three times using the freeze–vacuum–thaw method. The mixture was then preheated in an oil bath at 70 °C, and polymerization was allowed to proceed for 19 h prior to being terminated by exposure to air and quenching in liquid nitrogen. The mixture was concentrated under vacuum and the solid residue was dissolved in 3 ml dimethylformamide, followed by adding 300 ml diethyl ether to the solution and storing the mixture overnight in a refrigerator. The resulting precipitate was removed by filtration and dried under vacuum, yielding a white solid. Table 1 provides the yield, conversion and degree of polymerization data.

General preparation of polymer/metal cyanide complex composites

Ternary composites were prepared by mixing DI water solutions of $K[Au(CN)_2]$ (1.0 mM, 2 ml) or $K_2[Pt(CN)_4]$ (0.5 mM, 2 ml) with DI water solutions of **1** to **5** ($[\text{-}NH_3Cl] = 1.0$ mM, 2 ml) at room temperature ($[\text{-}NH_3] = [Au(CN)_2] = 1/2[Pt(CN)_4] = 0.5$ mM). Furthermore, when amphiphilic polymers were prepared at less than pH 9 (under amine-protonated conditions), the composites with metal complexes were prepared, indicating the electrostatic interaction between metal complexes and amphiphilic polymers with protonated amino terminal groups. All composite solutions prepared in this manner were found to be stable in oxygen-free DI water for a period of 1 month, although pure $K[Au(CN)_2]$ in DI water was unstable in air and decomposed, with the formation of both oxidation and hydrolysis products and with a concurrent loss of photoluminescence. The stabilization induced on adding the amphiphiles indicates that the aggregation of the composites subsequent to the polymer addition prevents $[Au(CN)_2]^-$ from reacting with oxygen.

RESULTS AND DISCUSSION

Supramolecular structures of DTC-NIPAAm$_n$-NH_3Cl with an alkyl and an amine group

DTC-NH_3Cl (Figure 1) was synthesized by introducing 1,2-diaminoethane to DTC, as in previous reports.[66–70] Amphiphilic PNIPAAm (DTC-PNIPAAm$_n$-NH_3Cl) was obtained by combining NIPAAm with DTC-NH_3Cl through RAFT polymerization (Table 1) to synthesize DTC-NIPAAm$_{13}$-NH_3Cl (**1**), DTC-NIPAAm$_{61}$-NH_3Cl (**2**), DTC-NIPAAm$_{78}$-NH_3Cl (**3**), DTC-NIPAAm$_{119}$-NH_3Cl (**4**) and DTC-NIPAAm$_{274}$-NH_3Cl (**5**) (Figure 1). Size-exclusion chromatography and ^1H NMR data indicate that each of the oligomers and polymers has a low polydispersity index, ranging from 1.03 to 1.20. When these amphiphilic polymers were dissolved in water at a concentration of 5 mM, transparent solutions were obtained. To study the thermal phase transitions at the LCST, the LCSTs of 5 mM aqueous solutions of these amphiphilic PNIPAAms were determined by turbidimetry, such that the transmittance of each solution was recorded while increasing its temperature. A slow heating rate of 0.2 °C min^{-1} was applied in all measurements to minimize the thermal lag between the sample cell and the solution. Table 2 summarizes the turbidimetry results for PNIPAAms **1–5** at different pH values. These data indicate that **1** has LCST values of 27, 28 and 30 °C at pH 9.0, 10.0 and 11.0, respectively, whereas no LCST is observed below pH 8.0. From these results, it is evident that aggregation and/or settling of the oligomers occurs owing to low solubility resulting from the deprotonation of the amine group. In contrast, **2–4** exhibit lower LCST values above pH 10.0 and an increase in M_n appears to elevate the LCST at pH 10.0 (**2**: 4 °C; **3**: 11 °C; **4**: 28 °C) and pH 11.0 (**2**: 4 °C; **3**: 14 °C; **4**: 27 °C). In addition, **5** shows a constant LCST in the vicinity of 30 °C despite changing the pH from 3.0 to 11.0. These results show that the end group effect of the amine moiety is more pronounced in the case of shorter chains. Moreover, the PNIPAAm chain effect is most significant for the high M_n sample **5**, whereas the end group effect is negligible in this sample. Therefore, the most important factors influencing the LCST are the hydrophilic amine group, the hydrophobic alkyl chain and the thermal transition of the PNIPAAm group.[71,72]

To examine the nanostructures of the amphiphilic NIPAAms in detail, TEM images of aqueous solutions of **1–5** at various pH values were acquired (Figure 2). Oligomer **1** displays a needle-like morphology (length: ~100 nm, width: ~3–5 nm) at pH 3.0 (Figure 2a), indicating that fibrous layers were formed as a result of its amphiphilic chemical structure. Using the Corey–Pauling–Koltun model (also referred to as space-filling calotte models)[73], the length of **1** was

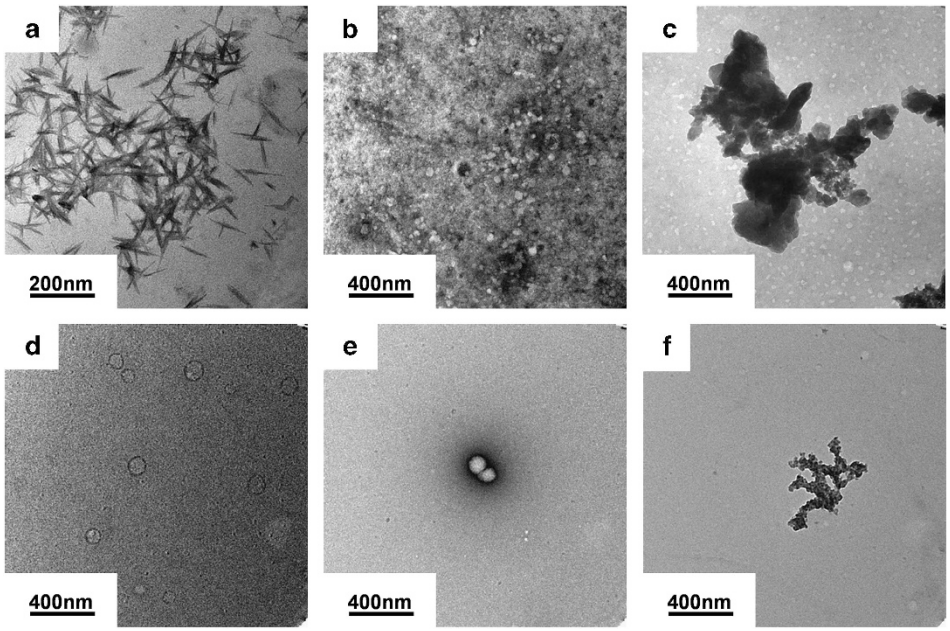

Figure 2 TEM images of DTC-NIPAAm$_n$-NH_3Cl samples in water (0.5 mM). (**a**) DTC-NIPAAm$_{13}$-NH_3Cl at pH 3.0, (**b**) DTC-NIPAAm$_{13}$-NH_3Cl at pH 7.0, (**c**) DTC-NIPAAm$_{13}$-NH_3Cl at pH 10.0, (**d**) DTC-NIPAAm$_{61}$-NH_3Cl at pH 3.0, (**e**) DTC-NIPAAm$_{61}$-NH_3Cl at pH 7.0, and (**f**) DTC-NIPAAm$_{61}$-NH_3Cl at pH 10.0. Samples were stained by 2 wt% uranyl acetate solution after casting and drying.

Table 3 LCST (°C) of amphiphilic NIPAAm (1–6) with $[Au(CN)_2]^-$ or $[Pt(CN)_4]^{2-}$ in aqueous solution at pH 7.0

Sample	*$[Au(CN)_2]^-$*	*$[Pt(CN)_4]^{2-}$*
1: DTC-NIPAAm$_{13}$-NH_3Cl	36	30
2: DTC-NIPAAm$_{61}$-NH_3Cl	38	30
3: DTC-NIPAAm$_{78}$-NH_3Cl	44	30
4: DTC-NIPAAm$_{119}$-NH_3Cl	33	30
5: DTC-NIPAAm$_{274}$-NH_3Cl	31	30

Abbreviations: DTC, *S*-1-dodecyl-*S*′-trithiocarbonate; LCST, lower critical solution temperature; NIPAAm, *N*-isopropylacrylamide.

estimated to be approximately 3 nm, assuming an all-*trans* configuration; hence, the width of the needle structures seen in the TEM images is nearly twice the length of the oligomer. These structures are therefore composed of bilayer strands and/or stacked multilayers of oligomers. In solutions with pH values >7.0, undefined or precipitated structures are observed (Figures 2b and c), indicating that the amine group was deprotonated and thus there was a lack of amphiphilicity. In addition, oligomer **2** displays a vesicle structure with a thickness of approximately 20 nm and a diameter of 100–150 nm at pH values of 3 and 7 (Figures 2d and e) but exhibits an agglomerated structure above pH 10.0 (Figure 2f). Conversely, **3**–**5** does not adopt any special morphologies. Generally, the colloidal micelles or vesicles formed by the amphiphilic NIPAAm polymers were found to be stable, and these supramolecular assemblies did not precipitate from water at elevated temperatures.[25,74,75] Thus the supramolecular assembly of **1** and **2** not only allows the tuning of the LCST but also leads to the formation of nanostructures in water.

Composites of amphiphilic NIPAAm oligomers and polymers with metal cyanide complexes

Dispersions were produced by adding $K[Au(CN)_2]$ or $K_2[Pt(CN)_4]$ to aqueous solutions of the amphiphilic NIPAAm polymers at 1:1 molar ratios (based on $[Au(CN)_2]^-$) or at 2:1 molar ratios (based on $[Pt(CN)_4]^{2-}$) relative to the amine moiety. The LCSTs of the final mixtures of these composites with amphiphilic PNIPAAms ($[PNIPAAm] = 5$ mM) were determined by turbidimetry. Table 3 summarizes the turbidimetry results for each PNIPAAm (**1**–**5**) when combined with $[Au(CN)_2]^-$ or $[Pt(CN)_4]^{2-}$, indicating that each composite exhibits a higher LCST than the original oligomer or polymer. It is known that, in general, the transition temperature and discontinuity exhibited by PNIPAAm gels are strongly affected by the presence of specific anions, such that the LCST is lowered.[76] Therefore, these results indicate that the aggregation of the oligomers and polymers is due to increased hydrophobic interactions and reduced solubility caused by the cancellation of electrostatic charges.

The associated aggregation and self-assembly of the metal cyanide complexes were investigated by TEM. In these experiments, the samples were not stained, and the dark regions are ascribed to Au or Pt present in the composites. Interestingly, **1**/$[Au(CN)_2]$ (Figure 3a) exhibits square nanostructures with widths in the range of 100–200 nm. In addition, **2**/$[Au(CN)_2]$ (Figure 3b), **1**/$[Pt(CN)_4]$ (Figure 4a) and **2**/$[Pt(CN)_4]$ (Figure 4b) adopt supramolecular nanostructures consisting of assembled nanorods (**2**/$[Au(CN)_2]$: length: 40–150 nm, width: 15–30 nm; **1**/$[Pt(CN)_4]$: length: 40–50 nm, width: 10–20 nm; **2**/$[Pt(CN)_4]$: length: 50–150 nm, width: 15–20 nm). These square and rod-like nanostructures presumably formed as a result of the self-assembly of metal complex/amphiphile composites. Diblock copolymers containing hydrophilic and hydrophobic chains tend to form unidirectionally stacked lamellar structures owing to the nucleation of lamellar layers, and when grown anisotropically, these lamellar layers generate nanorods.[23–25] These amphiphilic PNIPAAms in combination with metal complexes are therefore capable of interacting not only at the molecular level but also on the nanometer scale to form hierarchical structures, a phenomenon similar to the formation of quaternary structures of proteins.

In contrast, composites of **3**–**5** with $[Au(CN)_2]$ or $[Pt(CN)_4]$ display either undefined or networked structures ranging from several hundred nanometers to several micrometers in length (Figures 3c–e

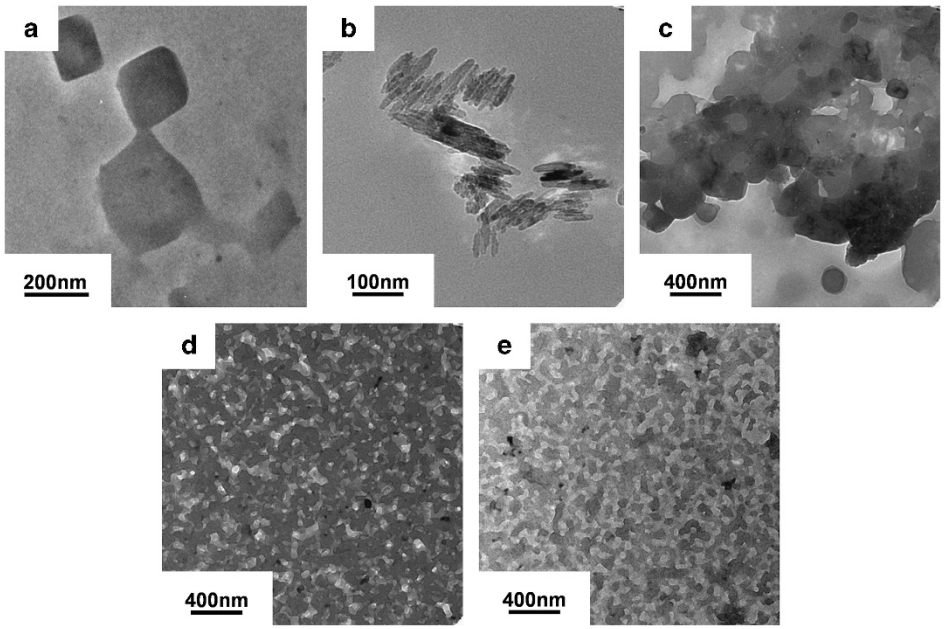

Figure 3 TEM images of DTC-NIPAAm$_n$-NH$_3$/[Au(CN)$_2$] samples in water at pH 7.0 ([**1**]=[**2**]=[**3**]=[**4**]=[**5**]=[Au(CN)$_2$]=0.5 mM). (**a**) **1**/[Au(CN)$_2$], (**b**) **2**/[Au(CN)$_2$], (**c**) **3**/[Au(CN)$_2$], (**d**) **4**/[Au(CN)$_2$] and (**e**) **5**/[Au(CN)$_2$]. Samples were observed without negative staining.

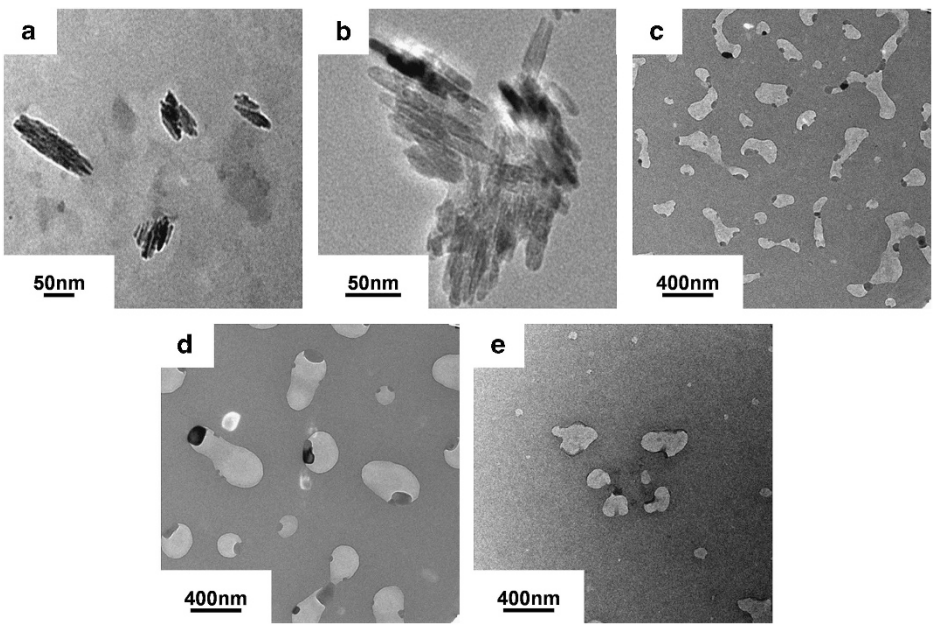

Figure 4 TEM images of DTC-NIPAAm$_n$-NH$_3$/[Pt(CN)$_4$] samples in water at pH 7.0 ([**1**]=[**2**]=[**3**]=[**4**]=[**5**]=1/2[Pt(CN)$_4$]=0.5 mM). (**a**) **1**/[Pt(CN)$_4$], (**b**) **2**/[Pt(CN)$_4$], (**c**) **3**/[Pt(CN)$_4$], (**d**) **4**/[Pt(CN)$_4$] and (**e**) **5**/[Pt(CN)$_4$]. Samples were observed without negative staining.

and 4c–e). Although it is possible that both the irregular and agglomerated structures were formed during sample preparation as a result of evaporation on the carbon-coated Cu mesh, it is more likely that these nanostructures were randomly generated as a consequence of the assembly of partially amorphous polymers into larger structures, in association with random-coil copolymers with higher degrees of polymerization.

The size distributions of the nanostructures in water were also analyzed by dynamic light scattering (DLS). DLS data were obtained for **1**–**5**/[Au(CN)$_2$] and **1**–**5**/[Pt(CN)$_4$] at 25 °C. The data of **1** with metal cyanide complexes contains at least two peaks in the volume-based mean nanostructure size distributions, at approximately 50 and 500 nm (Figures 5a and 6a). These results are consistent with the square and rod nanostructures having thicknesses of the order of tens of nanometers and widths of the order of several hundreds of nanometers observed in the TEM images, although DLS only evaluates the hydrodynamic radii of dispersed structures in a solvent. PNIPAAm **2** with metal cyanide complexes also shows a light scattering signal indicating several hundred nanometers (Figures 5b and 6b). In contrast, **3**–**5** with metal cyanide complexes show light scattering signals with at least three peaks in the volume-based mean size distributions, at approximately several tens of nanometers, several

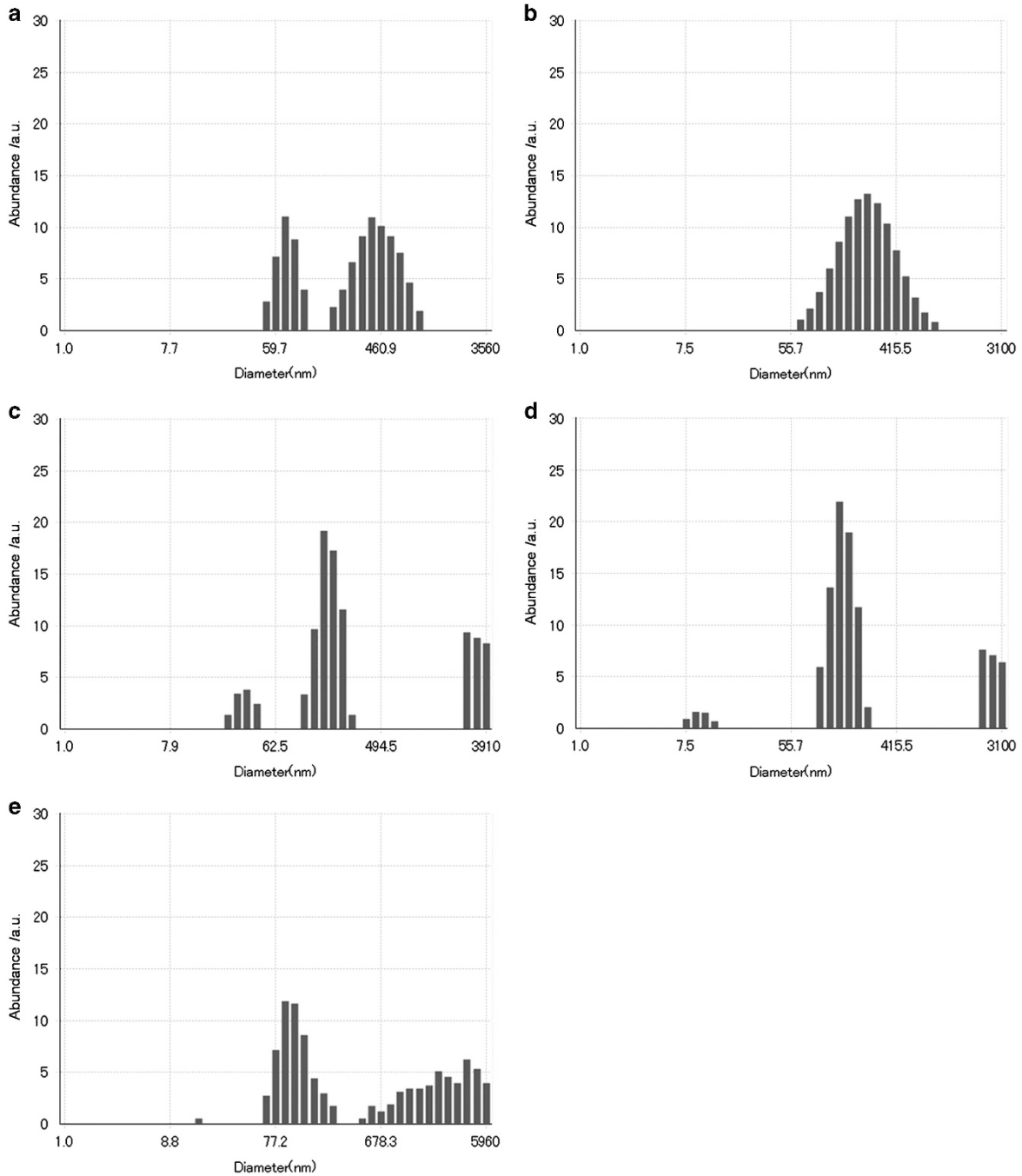

Figure 5 Size distributions of DTC-NIPAAm$_n$-NH$_3$/[Au(CN)$_2$] samples in water at pH 7.0 ([**1**]=[**2**]=[**3**]=[**4**]=[**5**]=[Au(CN)$_2$]=0.5 mM). (**a**) **1**/[Au(CN)$_2$], (**b**) **2**/[Au(CN)$_2$], (**c**) **3**/[Au(CN)$_2$], (**d**) **4**/[Au(CN)$_2$] and (**e**) **5**/[Au(CN)$_2$].

hundreds of nanometers and several microns (Figures 5c–e and 6c–e), which are consistent with the multi-dispersed assemblies in the TEM images. The results demonstrate that the use of amphiphilic NIPAAm/metal cyanide complexes leads to the assembly of supramolecular structures in water.

SAXS analysis of the composites in water was performed (Figures 7a and b), and SAXS profiles were generated from isotropic 2-D SAXS patterns. The results show the formation of cylindrical nanostructures with sizes ranging from several nanometers to ~20–70 nm, determined by fitting the data with a cylindrical model for a mixture of cylinders with different radii (Figures 7c–g). The lengths of all oligomers and polymers were estimated to be ~3–5 nm, assuming an all-*trans* configuration using the Corey–Pauling–Koltun model (also referred to as space-filling calotte models)[73]. The size of the structures, ~20–70 nm, was approximately several times the length of the oligomer. In addition, it is noteworthy that the model consisting of a mixture of spheres can also be used to fit the data (Supplementary Figure S1), whereas the lamellar model consisting of a mixture of lamellae with different thicknesses cannot be used to sufficiently fit the data (Supplementary Figure S2). Therefore, based on the complementary TEM, DLS and SAXS data, it is suggested that hybrids of PNIPAAms and metal complexes can lead not only to

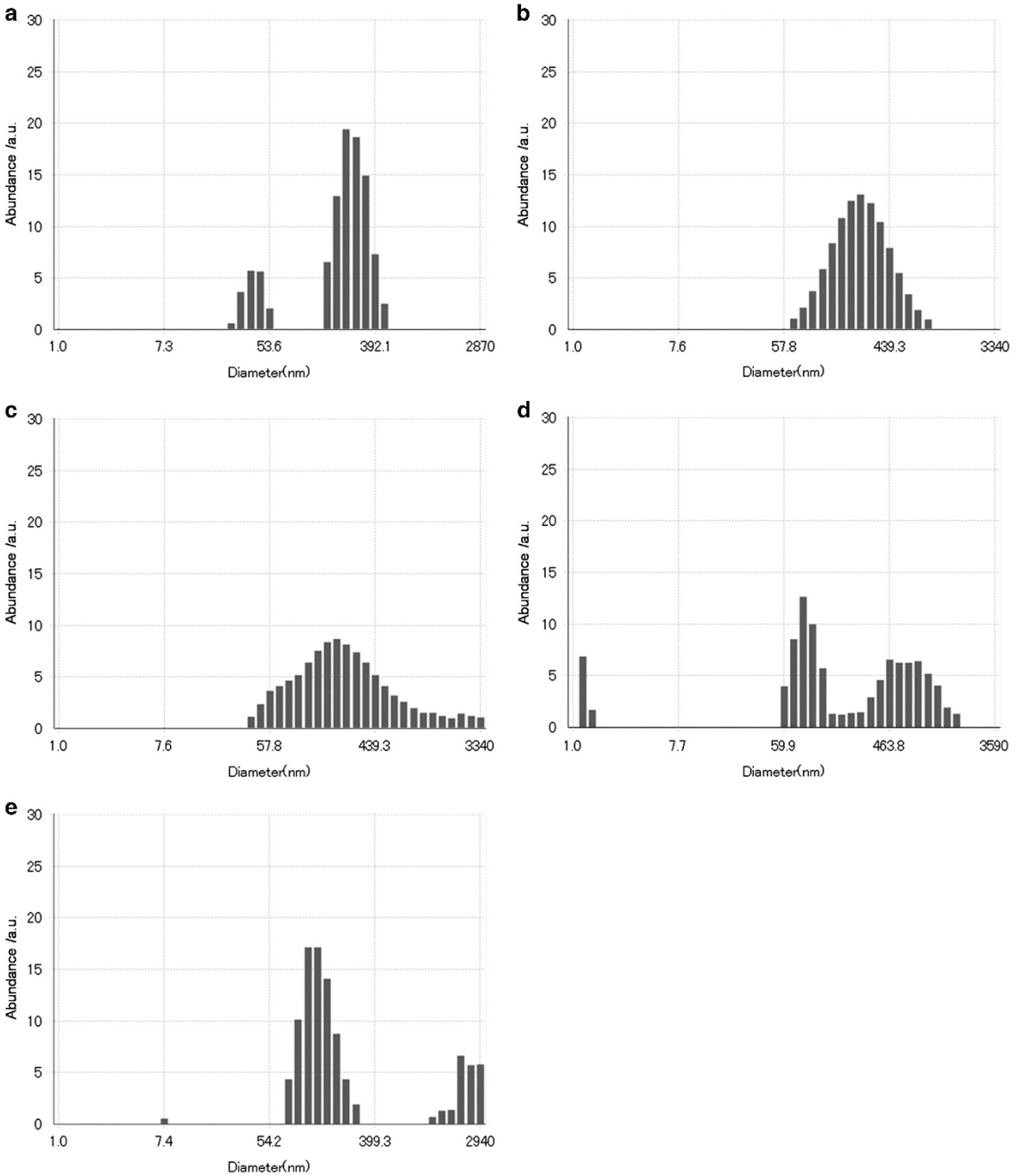

Figure 6 Size distributions of DTC-NIPAAm$_n$-NH$_3$/[Pt(CN)$_4$] samples in water at pH 7.0 ([**1**] = [**2**] = [**3**] = [**4**] = [**5**] = 1/2[Pt(CN)$_4$] = 0.5 mM). (**a**) **1**/[Pt(CN)$_4$], (**b**) **2**/[Pt(CN)$_4$], (**c**) **3**/[Pt(CN)$_4$], (**d**) **4**/[Pt(CN)$_4$] and (**e**) **5**/[Pt(CN)$_4$].

nanostructures in water but also to cylindrical aggregates with radii of ~20–70 nm (or spherical aggregates of the order of several nanometers in size) assembled in rod, square and sheet structures with widths of several hundred nanometers.

Nanocomposites of these amphiphilic oligomers/polymers with $[Au(CN)_2]^-$ or $[Pt(CN)_4]^{2-}$ were also assessed by UV-vis spectroscopy (Supplementary Figure S3). The addition of 0.5 mM aqueous solutions of K[Au(CN)$_2$] to **1**–**5** results in the appearance of a new absorption shoulder and/or peaks in the region of 250–350 nm. These observations suggest the presence of $[Au(CN)_2]^-$ and $[Pt(CN)_4]^{2-}$, which both exhibit electrostatic interactions with the positively charged amine moieties of the NIPAAm and metallophilicity. We also investigated the aggregation of $[Au(CN)_2]^-$ and $[Pt(CN)_4]^{2-}$ and their metallophilic interactions by obtaining luminescence spectra of the composites. The emission spectra of composites **1**–**5**/$[Au(CN)_2]^-$ (amine group:K[Au(CN)$_2$] = 1:1) and **1**–**5**/$[Pt(CN)_4]^{2-}$ (amine group: [Pt(CN)$_4$] = 2:1) are shown in Supplementary Figure S4. The 0.5 mM solutions of $[Au(CN)_2]^-$ and $[Pt(CN)_4]^{2-}$ exhibit weak luminescence in the range of 340–450 nm. However, the quantum yields of $[Au(CN)_2]^-$ and $[Pt(CN)_4]^{2-}$ in DI water are both $<1\%$, and the emission lifetimes of these solutions are <10 ns (Supplementary Table S1). These data suggest that almost all of the observed luminescence

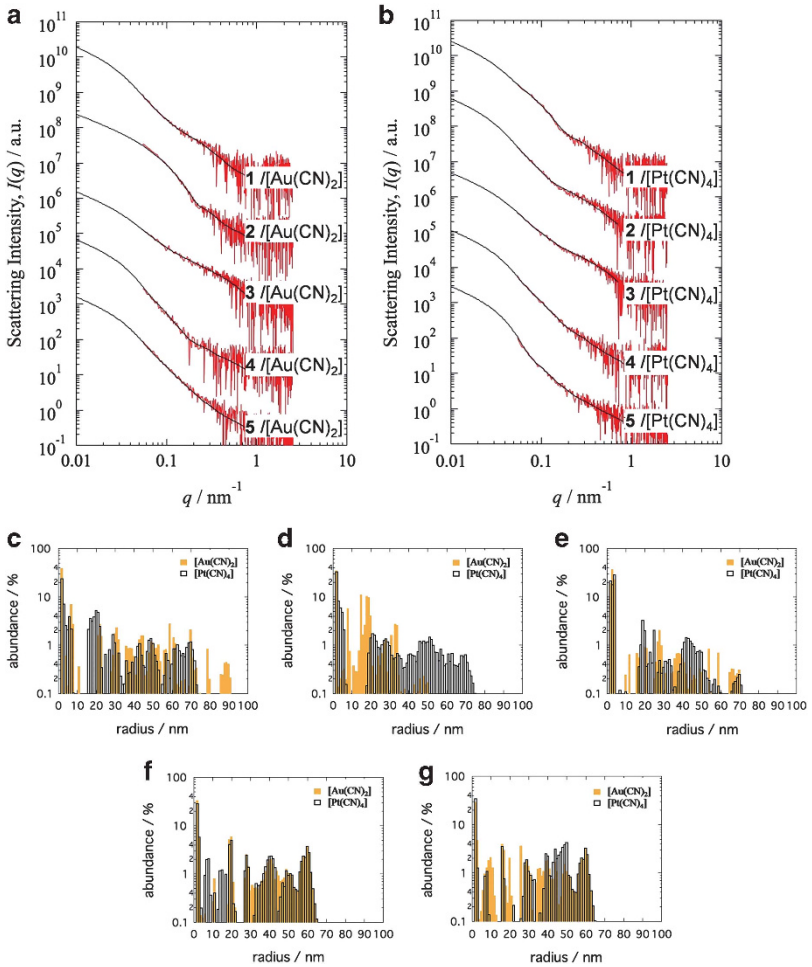

Figure 7 SAXS profiles (double logarithmic plot of the scattering intensity vs q) of (**a**) DTC-NIPAAm$_n$-NH$_3$/[Au(CN)$_2$] and (**b**) DTC-NIPAAm$_n$-NH$_3$/[Pt(CN)$_4$]. Evaluated size distributions, determined by fitting the SAXS profiles with the cylindrical model, for DTC-NIPAAm$_n$-NH$_3$/metal cyanide complexes in water at pH 7.0 ([**1**]=[**2**]=[**3**]=[**4**]=[**5**]=[Au(CN)$_2$]=1/2[Pt(CN)$_4$]=0.5 mM). (**c**) **1**/metal cyanide complexes, (**d**) **2**/metal cyanide complexes, (**e**) **3**/metal cyanide complexes, (**f**) **4**/metal cyanide complexes, and (**g**) **5**/metal cyanide complexes.

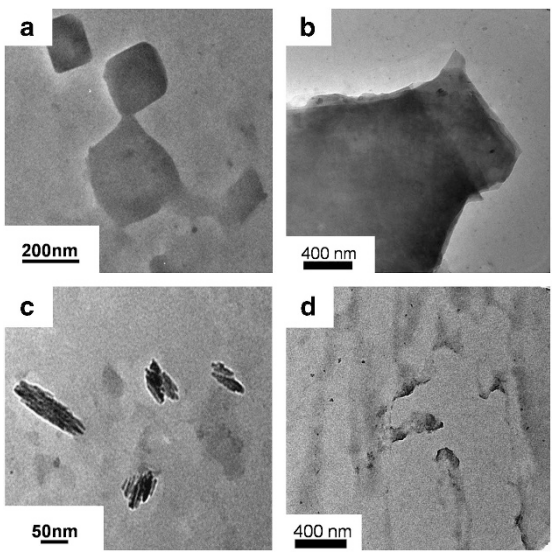

Figure 8 TEM images of DTC-NIPAAm$_{13}$-NH$_3$ (**1**)/[Au(CN)$_2$] samples at (**a**) 21 °C and (**b**) 45 °C and DTC-NIPAAm$_{13}$-NH$_3$/[Pt(CN)$_4$] at (**c**) 21 °C and (**d**) 45 °C in water at pH 7.0 ([**1**]=[Au(CN)$_2$]=1/2[Pt(CN)$_4$]=0.5 mM).

originates from the monomeric fluorescence of $[Au(CN)_2]^-$ and $[Pt(CN)_4]^{2-}$ previously observed in water,[77–79] although weak metallophilic interactions were observed in the luminescence spectra. Overall, based on solvation dynamics, it appears that composites of $[Au(CN)_2]^-$ or $[Pt(CN)_4]^{2-}$ with the amphiphilic oligomers/polymers undergo alignment such that there is sufficient distance between the metal complexes, even in the nanocomposites.

Thermoresponsive metallophilic interactions of amphiphilic NIPAAm/metal cyanide complexes

To confirm the relationship between thermoresponsiveness and morphology, Figure 8 displays a set of representative TEM images of samples prepared in solutions at different temperatures. At 21 °C, **1**/[Au(CN)$_2$] shows a square-like structure (Figure 8a). In contrast, at 45 °C, sheet-like structures appear (Figure 8b), resulting from the aggregation of the nanocomposite upon undergoing the LCST. The thermoresponsive nanocomposite **1**/[Au(CN)$_2$] thus undergoes assembly owing to the extension of the PNIPAAm chain and the small metal–metal distance. Below the LCST of the nanocomposite (30 °C), the interaction among PNIPAAm chains is weak. It is noted that, above the LCST, 2-D sheets with widths of several microns are self-assembled with increasing temperature. In the case of **1**/[Pt(CN)

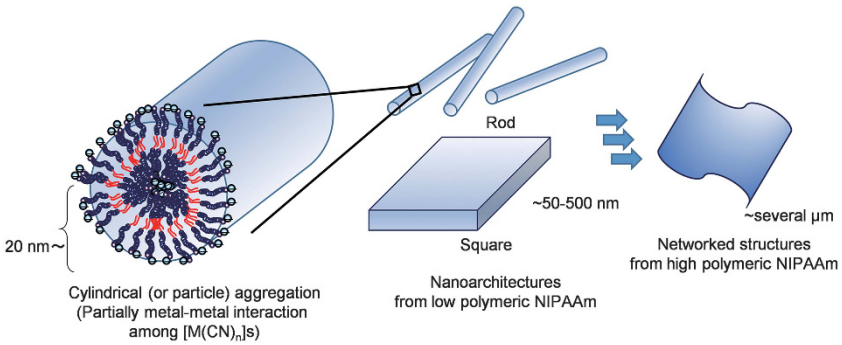

Figure 9 Hierarchical schematic illustration of the self-assembly of DTC-NIPAAm$_n$-NH$_3$/[Au(CN)$_2$] and DTC-NIPAAm$_n$-NH$_3$/[Pt(CN)$_4$] in water.

$_4$], thermoresponsive interactions are also found (Figures 8c and d), while the self-assembling structures of the nanocomposites composed of **2**–**5** are fully agglomerated and TEM images do not show clear morphologies. Therefore, the thermoresponsive phenomenon is attributed to delicate interactions among the metal complexes via van der Waals forces between the chains of **1**. In contrast, nanocomposites containing **2**–**5**, which have longer PNIPAAm chains than **1**, exhibit interactions that are too strong to maintain assembled structures in water.

PNIPAAm is hydrophilic below the LCST but becomes hydrophobic following the LCS transition. Amphiphilic NIPAAm/metal cyanide complexes thus undergo phase transitions at their LCST because of the cooperative dehydration of the PNIPAAm chains and the concomitant collapse of individual chains from hydrated coils to hydrophobic globules. A second cause of phase transitions at the LCST is the weak metallophilic interactions among metal cyanide complexes. As a result of these two factors, the nanocomposites investigated herein show remarkable temperature sensitivity.

The results of our morphological and spectroscopic characterization provide detailed information regarding the nature of the composites self-assembled from diblock copolypeptide amphiphiles and metal complexes (Figure 9). The data from UV-vis absorption and luminescence analyses show that the amphiphilic PNIPAAm/metal cyanide composites include both aggregated and monomeric species. The electrostatic interactions between the amine segments and the anionic metal cyanide complexes as well as the low degree of polymerization of approximately 100 both have a significant role in the morphological control. High-resolution TEM observations demonstrate that molecular-scale rod structures are formed from the aggregation of the polymer with metal complexes, especially when employing PNIPAAm with lower degrees of polymerization. It is therefore evident that the amphiphile is capable of inducing interesting alignment structures in aqueous solutions of metal complexes.

CONCLUSIONS

We have demonstrated the formation of amphiphilic PNIPAAm/metal cyanide complex composites with significant variations in nanostructure depending on the structure of the PNIPAAm. The formation of composite materials produced by combining these amphiphiles with the metal complexes demonstrates that it is possible to promote the formation of one-dimensional structures such as rods as well as more complex architectures, including square structures. The technique of combining amphiphilic molecules with discrete coordination compounds thus makes it possible to design flexible supramolecular coordination systems. This general concept of an amphiphilic polymer composite could be extended to include other useful compounds and should provide valuable information leading to further advances in the fields of coordination materials and synthetic polymer chemistry.

CONFLICT OF INTEREST

The authors declare no conflict of interest.

ACKNOWLEDGEMENTS

This work was financially supported in part by a Grant-in-Aid for Young Scientists (A) (No. 24685019) and a Grant-in-Aid for Scientific Research on Innovative Areas (new polymeric materials based on element blocks, no. 2401) (Nos. 25102547 and 15H00770). SAXS measurements were performed at the Photon Factory of High Energy Accelerator Research Organization (Approval number 2013G507).

1 Gómez-Romero, P. & Sanchez, C. *Functional Hybrid Materials* (eds Gómez-Romero P. & Sanchez, C.) (Wiley-VCH: Weinheim, Germany, 2004).
2 Hirai, H., Chawanya, H. & Toshima, N. Colloidal palladium protected with poly(*N*-vinyl-2-pyrrolidinone) for selective hydrogenation of cyclopentadiene. *React. Polym. Ion Exchangers Sorbents* **3**, 127–141 (1985).
3 Hirai, H., Nakao, Y. & Toshima, N. Colloidal rhodium in poly(vinylpyrrolidone) as hydrogenation catalyst for internal olefins. *Chem. Lett.* **7**, 545–548 (1978).
4 Chujo, Y. & Saegusa, T. Organic polymer hybrids with silica gel formed by means of the sol-gel method. *Adv. Polym. Sci.* **100**, 11–29 (1992).
5 Chujo, Y., Ihara, E., Kure, S., Suzuki, K. & Saegusa, T. Block copolymer of 2-methyl-2-oxazoline with silica gel. An organic-inorganic hybrid polymer. *Makromol. Chem. Macromol. Symp.* **42/43**, 303–312 (1991).
6 Kim, S. & Bawendi, M. G. Oligomeric ligands for luminescent and stable nanocrystal quantum dots. *J. Am. Chem. Soc.* **125**, 14652–14653 (2003).
7 Gangopadhyay, R. & De, A. Conducting polymer nanocomposites: a brief overview. *Chem. Mater.* **12**, 608–622 (2000).
8 Thakur, V. K., Ding, G., Ma, J., Lee, P. S. & Lu, X. Hybrid materials and polymer electrolytes for electrochromic device applications. *Adv. Mater.* **24**, 4071–4096 (2012).
9 Gómez-Romero, P. Hybrid organic-inorganic materials-in search of synergic activity. *Adv. Mater.* **13**, 163–174 (2001).
10 Walcarius, A. Electrochemical applications of silica-based organic-inorganic hybrid materials. *Chem. Mater.* **13**, 3351–3372 (2001).
11 Gómez-Romero, P., Cuentas-gallegos, K., Lira-cantú, M. & Casañ-pastor, N. Hybrid nanocomposite materials for energy storage and conversion applications. *J. Mater. Sci.* **40**, 1423–1428 (2002).
12 Zhou, R. & Xue, J. Hybrid polymer-nanocrystal materials for photovoltaic applications. *Chem. Phys. Chem.* **13**, 2471–2480 (2012).
13 Holder, E., Tessler, N. & Rogach, A. L. Hybrid nanocomposite materials with organic and inorganic components for opto-electronic devices. *J. Mater. Chem.* **18**, 1064–1078 (2008).
14 Sessolo, M. & Bolink, H. J. Hybrid organic-inorganic light-emitting diodes. *Adv. Mater.* **23**, 1829–1845 (2011).
15 Jäekle, L. Advances in the synthesis of organoborane polymers for optical, electronic, and sensory applications. *Chem. Rev.* **110**, 3985–4022 (2010).
16 Zhao, L. & Lin, Z. Crafting semiconductor organic-inorganic nanocomposites via placing conjugated polymers in intimate contact with nanocrystals for hybrid solar cells. *Adv. Mater.* **24**, 4353–4368 (2012).
17 Watanabe, H., Vendamme, R. & Kunitake, T. Development of fabrication of giant nanomembranes. *Bull. Chem. Soc. Jpn* **80**, 433–440 (2007).
18 Watanabe, H. & Kunitake, T. A large, freestanding, 20 nm thick nanomembrane based on an epoxy resin. *Adv. Mater.* **19**, 909–912 (2007).

19 Chujo, Y. & Tanaka, K. New polymeric materials based on element-blocks. *Bull. Chem. Soc. Jpn* **88**, 633–643 (2015).
20 Kuroiwa, K., Yoshida, M., Masaoka, S., Kaneko, K., Sakai, K. & Kimizuka, N. Self-assembly of tubular microstructures from mixed-valence metal complexes and their reversible transformation by external stimuli. *Angew Chem. Int. Ed.* **51**, 656–659 (2012).
21 Kuroiwa, K. Dynamic self-assembly from mixed-valence metal complexes and their reversible transformations by external stimuli. *Kobunshi Ronbunshu* **69**, 485–492 (2012).
22 Kuroiwa, K. & Kimizuka, N. Self-assembly and functionalization of lipophilic metal-triazole complexes in various media. *Polym. J.* **45**, 384–390 (2013).
23 Kuroiwa, K., Arie, T., Sakurai, S., Hayami, S. & Deming, T. J. Supramolecular control of reverse spin transitions in cobalt(II) terpyridine complexes with diblock copolypeptide amphiphiles. *J. Mater. Chem. C* **3**, 7779–7783 (2015).
24 Kuroiwa, K., Masaki, Y., Koga, Y. & Deming, T. J. Self-assembly of discrete metal complexes in aqueous solution via block copolypeptide amphiphiles. *Int. J. Mol. Sci.* **14**, 2022–2035 (2013).
25 Kuroiwa, K., Higuma, C., Shimogawa, Y., Hachisako, H. & Sakurai, S. Development of amphiphilic n-isopropylacrylamide oligomers and polymers, and their composites with metal ions. *Kobunshi Ronbunshu* **71**, 457–466 (2014).
26 Heskins, M., Guillet, J. E. & James, E. Solution properties of poly(*N*-isopropylacrylamide). *J. Macromol. Sci. Chem.* **2**, 1441–1455 (1968).
27 Schild, H. G. Poly(*N*-isopropylacrylamide): experiment, theory and application. *Prog. Polym. Sci.* **17**, 163–249 1992)
28 Smithenry, D. W., Kang, M.-S. & Gupta, V. K. Telechelic poly(*N*-isopropylacrylamide): polymerization and chain aggregation in solution. *Macromolecules* **34**, 8503–8511 (2001).
29 Kujawa, P., Watanabe, H., Tanaka, F. & Winnik, F. M. Amphiphilic telechelic poly(*N*-isopropylacrylamide) in water: from micelles to gels. *Eur. Phys. J. E: Soft Matter* **17**, 129–137 (2005).
30 Kujawa, P., Segui, F., Shaban, S., Diab, C., Okada, Y., Tanaka, F. & Winnik, F. M. Impact of end-group association and main-chain hydration on the thermosensitive properties of hydrophobically modified telechelic poly(*N*-isopropylacrylamides) in water. *Macromolecules* **39**, 341–348 (2006).
31 Plummer, R., Hill, D. J. T. & Whittaker, A. K. Solution properties of star and linear poly (*N*-isopropylacrylamide). *Macromolecules* **39**, 8379–8388 (2006).
32 Housni, A. & Narain, R. Aqueous solution behavior of P(*N*-isopropyl acrylamide) in the presence of water-soluble macromolecular species. *Eur. Polym. J.* **43**, 4344–4354 (2007).
33 Yusa, S.-i., Yamago, S., Sugahara, M., Morikawa, S., Yamamoto, T. & Morishima, Y. Thermo-responsive diblock copolymers of poly(*N*-isopropylacrylamide) and poly(*N*-vinyl-2-pyrroridone) synthesized via organotellurium-mediated controlled radical polymerization (TERP). *Macromolecules* **40**, 5907–5915 (2007).
34 Shan, J., Zhao, Y., Granqvist, N. & Tenhu, H. Thermoresponsive properties of N-isopropylacrylamide oligomer brushes grafted to gold nanoparticles: effects of molar mass and gold core size. *Macromolecules* **42**, 2696–2701 (2009).
35 Nagai, A., Yoshii, R., Otsuka, T., Kokado, K. & Chujo, Y. BODIPY-based chain transfer agent: reversibly thermoswitchable luminescent gold nanoparticle stabilized by BODIPY-terminated water-soluble polymer. *Langmuir* **26**, 15644–15649 (2010).
36 Smith, A. E., Xu, X., Savin, D. A. & McCormick, C. L. Reversible gold "locked" synthetic vesicles derived from stimuli-responsive diblock copolymers. *Polym. Chem.* **1**, 628–630 (2010).
37 Lian, X., Jin, J., Tian, J. & Zhao, H. Thermoresponsive nanohydrogels cross-linked by gold nanoparticles. *ACS Appl. Mater. Interfaces* **2**, 2261–2268 (2010).
38 Liang, M., Lin, I.-C., Whittaker, M. R., Minchin, R. F., Monteiro, M. J. & Toth, I. Cellular uptake of densely packed polymer coatings on gold nanoparticles. *ACS Nano* **4**, 403–413 (2010).
39 Liu, Y., Tu, W. & Cao, D. Synthesis of gold nanoparticles coated with polystyrene-block-poly(*N*-isopropylacrylamide) and their thermoresponsive ultraviolet-visible absorbance. *Ind. Eng. Chem. Res.* **49**, 2707–2715 (2010).
40 Sistach, S., Beija, M., Rahal, V., Brulet, A., Marty, J.-D., Destarac, M. & Mingotaud, C. Thermoresponsive amphiphilic diblock copolymers synthesized by MADIX/RAFT: properties in aqueous solutions and use for the preparation and stabilization of gold nanoparticles. *Chem. Mater.* **22**, 3712–3724 (2010).
41 Ebeling, B. & Vana, P. RAFT-polymers with single and multiple trithiocarbonate groups as uniform gold-nanoparticle coatings. *Macromolecules* **46**, 4862–4871 (2013).
42 Li, W., Cai, X., Kim, C., Sun, G., Zhang, Y., Deng, R., Yang, M., Chen, J., Achilefu, S., Wang, L. V. & Xia, Y. Gold nanocages covered with thermally-responsive polymers for controlled release by high-intensity focused ultrasound. *Nanoscale* **3**, 1724–1730 (2011).
43 Sun, X.-L., He, W.-D., Li, J., He, N., Han, S.-C. & Li, L.-Y. Preparation of polypyrrole-graft-poly(*N*-isopropylacrylamide)/silver nanocomposites from pyrrolyl-capped macromonomer by $AgNO_3$ and their stimuli responsibility of light emission. *J. Polym. Sci. A Polym. Chem.* **46**, 6950–6960 (2008).
44 Li, Q., Zhang, L., Bai, L., Zhang, Z., Zhu, J., Zhou, N., Cheng, Z. & Zhu, X. Multistimuli-responsive hybrid nanoparticles with magnetic core and thermoresponsive fluorescence-labeled shell via surface-initiated RAFT polymerization. *Soft Matter* **7**, 6958–6966 (2011).
45 Wu, X., He, X., Zhong, L., Lin, S., Wang, D., Zhu, X. & Yan, D. Water-soluble dendritic-linear triblock copolymer-modified magnetic nanoparticles: preparation, characterization and drug release properties. *J. Mater. Chem.* **21**, 13611–13620 (2011).
46 Wang, H., Luo, W. & Chen, J. Fabrication and characterization of thermoresponsive Fe_3O_4@PNIPAM hybrid nanomaterials by surface-initiated RAFT polymerization. *J. Mater. Sci.* **47**, 5918–5925 (2012).
47 Budgin, A. M., Kabachii, Y. A., Shifrina, Z. B., Valetsky, P. M., Kochev, S. S., Stein, B. D., Malyutin, A. & Bronstein, L. M. Functionalization of magnetic nanoparticles with amphiphilic block copolymers: self-assembled thermoresponsive submicrometer particles. *Langmuir* **28**, 4142–4151 (2012).
48 You, Y.-Z., Kalebaila, K. K., Brock, S. L. & Oupický, D. Temperature-controlled uptake and release in PNIPAM-modified porous silica nanoparticles. *Chem. Mater.* **20**, 3354–3359 (2008).
49 Chen, J., Liu, M., Chen, C., Gong, H. & Gao, C. Synthesis and characterization of silica nanoparticles with well-defined thermoresponsive PNIPAM via a combination of RAFT and click chemistry. *ACS Appl. Mater. Interfaces* **3**, 3215–3223 (2011).
50 Xu, L., Pan, J., Xia, Q., Shi, F., Dai, J. i., Wei, X. & Yan, Y. Composites of silica and molecularly imprinted polymers for degradation of sulfadiazine. *J. Phys. Chem. C* **116**, 25309–25318 (2012).
51 Masuda, T., Yamamoto, S.-i., Moriya, O., Kashio, M. & Sugizaki, T. Preparation of amphiphilic polysilsesquioxane by grafting of block copolymer of acrylamide monomers. *Polym. J.* **39**, 220–229 (2007).
52 Zhang, W., Liu, L., Zhuang, X., Li, X., Bai, J. & Chen, Y. Synthesis and self-assembly of tadpole-shaped organic/inorganic hybrid poly(*N*-isopropylacrylamide) containing polyhedral oligomeric silsesquioxane via RAFT polymerization. *J. Polym. Sci. A: Polym. Chem.* **46**, 7049–7061 (2008).
53 Wang, L., Zeng, K. & Zheng, S. Hepta(3,3,3-trifluoropropyl) polyhedral oligomeric silsesquioxane-capped poly(*N*-isopropylacrylamide) telechelics: synthesis and behavior of physical hydrogels. *ACS Appl. Mater. Interfaces* **3**, 898–909 (2011).
54 Zhang, W., Wang, S., Li, X., Yuan, J. & Wang, S. Organic/inorganic hybrid star-shaped block copolymers of poly(l-lactide) and poly(*N*-isopropylacrylamide) with a polyhedral oligomeric silsesquioxane core: synthesis and self-assembly. *Eur. Polym. J.* **48**, 720–729 (2012).
55 Lehto, J., Vaaramaa, K., Vesterinen, E. & Tenhu, H. Uptake of zinc, nickel, and chromium by N-isopropyl acrylamide polymer gels. *J. Appl. Polym. Sci.* **68**, 355–362 (1998).
56 Zhang, L.-J., Cao, L.-Q., Wang, X.-H. & Wang, J.-D. Preparation of the thermosensitive metal ion imprinted polymer in supercritical carbon dioxide: application in the selective recognition of copper (II). *Polym. Adv. Technol.* **23**, 1174–1180 (2012).
57 Irie, M., Misumi, Y. & Tanaka, T. Stimuli-responsive polymers: chemical induced reversible phase separation of an aqueous solution of poly(*N*-isopropylacrylamide) with pendent crown ether groups. *Polymer* **34**, 4531–4535 (1993).
58 Kuckling, D. & Pareek, P. Synthesis of transition-metal-ion-selective poly(*N*-isopropylacrylamide) hydrogels by the incorporation of an aza crown ether. *J. Polym. Sci. A Polym. Chem.* **41**, 1594–1602 (2003).
59 Chayama, K., Morita, Y. & Iwatsuki, S. Thermosensitive gels incorporating polythioether units for the selective extraction of class B metal ions. *J. Chromatogr. A* **1217**, 6785–6790 (2010).
60 Liu, T., Hu, J., Yin, J., Zhang, Y., Li, C. & Liu, S. Enhancing detection sensitivity of responsive microgel-based Cu(II) chemosensors via thermo-induced volume phase transitions. *Chem. Mater.* **21**, 3439–3446 (2009).
61 Chiper, M., Fournier, D., Hoogenboom, R. & Schubert, U. S. Thermosensitive and switchable terpyridine-functionalized metallo-supramolecular poly(*N*-isopropylacrylamide). *Macromol. Rapid Commun.* **29**, 1640–1647 (2008).
62 Qin, L., He, X.-W., Zhang, W., Li, W.-Y. & Zhang, Y.-K. Macroporous thermosensitive imprinted hydrogel for recognition of protein by metal coordinate interaction. *Anal. Chem.* **81**, 7206–7216 (2009).
63 Alexandridis, P. & Lindman, B. *Amphiphilic Block Copolymers. Self-Assembly and Applications* (eds Alexandridis, P. & Lindman, B.) (Elsevier, Amsterdam, The Netherlands, 2000).
64 Nagarajan, R. *Amphiphiles Molecular Assembly and Applications* (ed Nagarajan, R.) (Oxford Univ. Press, Oxford, UK, 2012).
65 Tien, N.-D., Sasaki, S., Masunaga, H., Shimizu, N., Igarashi, N. & Sakurai, S. Small-angle X-ray scattering studies on melting and recrystallization behaviors of poly (oxyethylene) crystallites in poly(D,L-lactide)/poly(oxyethylene) blends. *Polymer* **55**, 2562–2569 (2014).
66 Lai, J. T., Filla, D. & Shea, R. Functional polymers from novel carboxyl-terminated trithiocarbonates as highly efficient RAFT agents. *Macromolecules* **35**, 6754–6756 (2002).
67 Zhang, X., Li, J., Li, W. & Zhang, A. Synthesis and characterization of thermo- and pH-responsive double-hydrophilic diblock copolypeptides. *Biomacromolecules* **8**, 3557–3567 (2007).
68 Wang, R., McCormick, C. L. & Lowe, A. B. Synthesis and evaluation of new dicarboxylic acid functional trithiocarbonates: RAFT synthesis of telechelic poly(n-butyl acrylate)s. *Macromolecules* **38**, 9518–9525 (2005).
69 Bouchékif, H. & Narain, R. Reversible addition-fragmentation chain transfer polymerization of *N*-isopropylacrylamide: a comparison between a conventional and a fast initiator. *J. Phys. Chem. B* **111**, 11120–11126 (2007).
70 Vega-Rios, A. & Licea-Claveríe, A. Controlled synthesis of block copolymers containing n-isopropylacrylamide by reversible addition-fragmentation chain-transfer (RAFT) polymerization. *J. Mex. Chem. Soc.* **55**, 21–32 (2011).
71 Xia, Y., Burke, N. A. D. & Stöver, H. D. H. End group effect on the thermal response of narrow-disperse poly(*N*-isopropylacrylamide) prepared by atom transfer radical polymerization. *Macromolecules* **39**, 2275–2283 (2006).

72 Nuopponen, M., Ojala, J. & Tenhu, H. Aggregation behaviour of well defined amphiphilic diblock copolymers with poly(*N*-isopropylacrylamide) and hydrophobic blocks. *Polymer* **45**, 3643–3650 (2004).
73 Corey, R. B. & Pauling, L. Molecular models of amino acids, peptides, and proteins. *Rev. Sci. Instrum.* **24**, 621–627 (1953).
74 Feil, H., Bae, Y. H., Feijen, J. & Kim, S. W. Effect of comonomer hydrophilicity and ionization on the lower critical solution temperature of *N*-isopropylacrylamide copolymers. *Macromolecules* **26**, 2496–2500 (1993).
75 Park, T. G. & Hoffman, A. S. Sodium chloride-induced phase transition in nonionic poly(*N*-isopropylacrylamide) gel. *Macromolecules* **26**, 5045–5048 (1993).
76 Suzuki, A. Phase transition in gels of sub-millimeter size induced by interaction with stimuli. *Adv. Polym. Sci.* **110**, 199–240 (1993).
77 Rawashdeh-Omary, M. A., Omary, M. A. & Patterson, H. H. Oligomerization of $Au(CN)_2^-$ and $Ag(CN)_2^-$ ions in solution via ground-state aurophilic and argentophilic bonding. *J. Am. Chem. Soc.* **122**, 10371–10380 (2000).
78 Yersin, H. Energy transfer from linear stacks of tetracyanoplatinates(II) to rare earth ions. *J. Chem. Phys.* **68**, 4707–4713 (1978).
79 Rawashdeh-Omary, M. A., Omary, M. A., Patterson, H. H. & Fackler, J. P. Jr. Excited-state interactions for $[Au(CN)_2^-]_n$ and $[Ag(CN)_2^-]_n$ oligomers in solution. Formation of luminescent gold-gold bonded excimers and exciplexes. *J. Am. Chem. Soc.* **123**, 11237–11247 (2001).

Supplementary Information accompanies the paper on Polymer Journal website (http://www.nature.com/pj)